ACS APPLIED MATERIALS & INTERFACES

Research Article

www.acsami.org

Rational Design and Facial Synthesis of $Li_3V_2(PO_4)_3$@C Nanocomposites Using Carbon with Different Dimensions for Ultrahigh-Rate Lithium-Ion Batteries

Wen-feng Mao,*[,†,‡] Yan-bao Fu,[†] Hui Zhao,[†] Guo Ai,[†] Yi-ling Dai,[†] Dechao Meng,[‡] Xin-he Zhang,[§] Deyang Qu,[§] Gao Liu,[†] Vincent S. Battaglia,[†] and Zhi-yuan Tang[‡]

[†]Energy and Environmental Technologies Division, Lawrence Berkeley National Laboratory, Berkeley, California 94720, United States

[‡]Department of Applied Chemistry, School of Chemical and Engineering, Tianjin University, Tianjin 300072, P. R. China

[§]McNair Technology Company, Ltd., Dongguan, Guangdong 523700, China

Supporting Information

ABSTRACT: $Li_3V_2(PO_4)_3$ (LVP) particles dispersed in different inorganic carbons (LVP@C) have been successfully synthesized via an in situ synthesis method. The inorganic carbon materials with different dimensions including zero-dimensional Super P (SP) nanospheres, one-dimensional carbon nanotubes (CNTs), two-dimensional graphene nanosheets, and three-dimensional graphite particles. The effects of carbon dimensions on the structure, morphology, and electrochemical performance of LVP@C composites have been systematically investigated. The carbon materials can maintain their original morphology even after oxidation (by NH_4VO_3) and high-temperature sintering (850 °C). LVP@CNT exhibits the best electrochemical performances among all of the samples. At an ultrahigh discharge rate of 100C, it presents a discharge capacity of 91.94 mAh g^{-1} (69.13% of its theoretical capacity) and maintains 79.82% of its original capacity even after 382 cycles. Its excellent electrochemical performance makes LVP@CNT a promising cathode candidate for lithium-ion batteries.

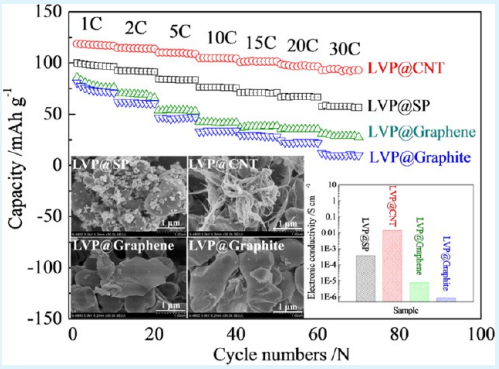

KEYWORDS: *lithium−vanadium phosphate, inorganic carbon, lithium-ion battery, cathode*

1. INTRODUCTION

Lithium-ion batteries (LIBs) have been well-known as promising energy storage devices for hybrid electric vehicles (HEVs) and electric vehicles (EVs).[1,2] However, many problems still exist in its practical application, such as low safety, high price, and low power density. Cathode material is a determining factor in LIBs, and it is urgent to develop novel cathode materials with high energy and power, high thermal stability, and low cost.[3,4]

Among all of the cathode candidates, monoclinic lithium−vanadium phosphate, $Li_3V_2(PO_4)_3$ (LVP), has attracted extensive attention because of its high operating voltage, large theoretical specific capacity, and thermodynamically stable structure.[5−21] However, the practical application of LVP has been limited by its inferior electronic conductivity because of the two separated [VO_6] octahedral arrangement.[22,23] Various strategies have been adopted to overcome this problem: (1) Doping with metal ions.[14,24,25] Although the conductivity can be increased in some degree, introducing guest atoms into the crystal lattices of LVP may also be deleterious and not easy to control via this method. (2) Reducing the particle size.[22,23,26] According to the diffusion formula $t = L^2/2D$ (where t is the diffusion time, L is the diffusion distance, and D is the diffusion coefficient), decreasing the particle size can significantly shorten the diffusion distance length, resulting in a fast Li^+-ion transfer in LVP, thus much enhancing its power performance. However, there exist many problems for nanosize cathode materials, such as low volume density and difficulty in mass production. (3) Coating with electrochemical conductive materials,[9,11,22,26] especially coating carbon. Although this method has been widely used for improving the electronic conductivity of electrode materials, perfect surface coatings are very difficult to achieve and a thicker coating layer may hinder Li^+-ion diffusion.

As we all know, some inorganic carbons have excellent properties: Super P (SP), a zero-dimensional (0D) carbon structure, has been widely used as conductive additive in LIBs and shows high electrochemical conductivity;[27] carbon nanotube (CNT), with one-dimensional (1D) carbon structure, exhibits exceptional electronic and mechanical properties;[28] graphene, a two-dimensional (2D) carbon structure, is of great

Received: March 13, 2015
Accepted: May 20, 2015
Published: May 20, 2015

DOI: 10.1021/acsami.5b02242
ACS Appl. Mater. Interfaces 2015, 7, 12057−12066

interest because of its high electric conductivity, large specific surface area, and excellent chemical/mechanical stability;[29] three-dimensional (3D) graphite has been widely used as a commercial anode material for LIBs.[30] Although these carbon materials have been widely investigated, there are no reports about using them as both carbon sources and reducing agents to synthesize LVP@C composites. Furthermore, the carbon dimensions on the electrochemical performance of LVP have never been reported before.

Herein, we introduced a facial route to synthesize LVP@C composites using the four inorganic carbons as both reducing agents and carbon sources. The effect of the carbon dimensions on the electrochemical performance of LVP has been carefully investigated. The synthesized LVP has a microparticle size and is uniformly dispersed in the carbon matrix. Among all of the LVP@C composites, the LVP@CNT composite maintains the highest electronic conductivity ($\sim 10^{-2}$ S cm^{-1}) and ionic conductivity, which makes it exhibit the best electrochemical performance (91.94 mAh g^{-1} can be obtained at an extra high rate of 100C). Compared with the same rate and a comparable loading, such a good electrochemical performance of LVP has never been reported.

2. EXPERIMENTAL SECTION

The LVP@C composite uses SP (denoted as LVP@SP) as the reducing agent, and the carbon source was synthesized via an ultrasonic-assisted sol−gel route. First, NH_4VO_3, $LiH_2(PO_4)_3$, and oxalic acid dihydrate in a stoichiometric ratio of 2:3:2 were dissolved in deionized water and magnetically stirred at room temperature until a clear yellow solution formed. Oxalic acid was employed as a chelating reagent. Then SP powders were added into the solution, and the mixture was treated ultrasonically for 2 h to disperse the SP nanospheres. The water was evaporated at 80 °C under stirring. The remaining solid was ground manually for 10 min, preheated at 350 °C for 4 h, and sintered at 850 °C for 8 h in a N_2 atmosphere to obtain the LVP@SP composites. The LVP@C composites use CNT, graphene, and graphite (denoted as LVP@CNT, LVP@Graphene, and LVP@Graphite) as reducing agents, and the carbon sources were prepared using a similar procedure by replacing the SP with CNT, graphene, or graphite.

The crystalline structures of the samples were examined by X-ray diffraction (XRD; Rigaku D/max 2500v/pc) using Cu Kα radiation. The particle morphology and microstructure of the composite were obtained using scanning electron microscopy (SEM; Philips XL30ESEM) and transmission electron microscopy (TEM; JEM-2100F). The particle size distributions of the composites were measured via a Delsa Nano C particle analyzer. The four-point probe resistivity measurement system is used to measure the electronic conductivities of the four composites.

The electrochemical tests were performed using 2032 coin-type cells composed of the cathode, lithium metal anode, a Celgard 2300 separator, and $LiPF_6$ in 1:1 ethylene carbonate/diethyl carbonate as the electrolyte. The cathode was fabricated by mixing 80% LVP@C composites with 10% acetylene black and 10% poly(vinylidene difluoride). The active material loading was about 2.5 mg cm^{-2}, and the diameter of the electrode was 10 mm. All cells were assembled in an argon-filled glovebox and then charged and discharged on a LISUN-CBT-138-32 multichannel battery test system in the potential range of 3.0−4.3 V. Cyclic voltammetry (CV) tests were carried out on a CHI1040B voltammeter with a potential range of 3.0−4.5 V. Electrochemical impedance spectroscopy measurements were carried out using a GAMRY electrochemical workstation in the frequency range of 10 kHz to 10 mHz with an alternating-current voltage of 5 mV.

3. RESULTS AND DISCUSSION

Figure 1 shows the XRD patterns of LVP@SP, LVP@CNT, LVP@Graphene, and LVP@Graphite. All diffraction peaks are

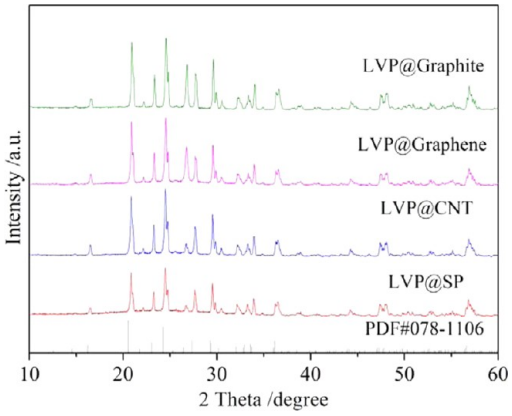

Figure 1. XRD patterns of LVP@SP, LVP@CNT, LVP@Graphene, and LVP@Graphite.

Table 1. Cell Parameters of LVP@SP, LVP@CNT, LVP@Graphene, and LVP@Graphite

sample	cell parameter			
	a (Å)	*b* (Å)	*c* (Å)	*V* (Å^3)
LVP@SP	8.612	12.070	8.634	897.52
LVP@CNT	8.604	12.060	8.630	895.48
LVP@Graphene	8.592	12.070	8.624	894.46
LVP@Graphite	8.581	12.060	8.616	891.45
PDF 078-1106	8.562	12.005	8.612	885.20

indexed to the monoclinic LVP phase (space group: $P21/n$), indicating that the high purity of all as-synthesized samples and the carbon types do not affect to the LVP structure. According to Rietveld refinement, the unit cell parameters were calculated (as noted in Table 1) and are in good agreement with the PDF 078-1106. On the basis of the weight difference of the composite before and after oxidization in air at 600 °C, the contents of carbon in LVP@SP, LVP@CNT, LVP@Graphene, and LVP@Graphite are 8.18, 8.22, 8.13, and 8.32 wt %, respectively, which indicates that the carbon contents in the four samples are almost the same.

The morphologies and schematic illustrations of LVP@SP, LVP@CNT, LVP@Graphene, and LVP@Graphite are displayed in Figure 2. It can be clearly seen that all of the samples have loose porous morphology. Especially, the LVP particles in the four samples exhibit the same regular globoid shapes, micrometer particle sizes, and smooth surfaces. The 0D SP nanospheres (Figure 2a,b), 1D CNT nanotubes (Figure 2d,e), 2D graphene nanosheets (Figure 2g,h), and 3D graphite particles (Figure 2j,k) maintain their original morphologies even after oxidation (by NH_4VO_3) and high-temperature sintering (850 °C). What is more, the SP, CNT, graphene, and graphite are uniformly dispersed without agglomerations because of the ultrasonic processing in the synthesis process, and the LVP particles are homogeneously dispersed in SP, CNT, graphene, and graphite networks. The LVP@C composites exhibit two notable features: First is the improvement in both the electronic and mechanical connection between the LVP particle and carbon material. This is the benefit from the in situ synthesized method in which inorganic

DOI: 10.1021/acsami.5b02242
ACS Appl. Mater. Interfaces 2015, 7, 12057−12066

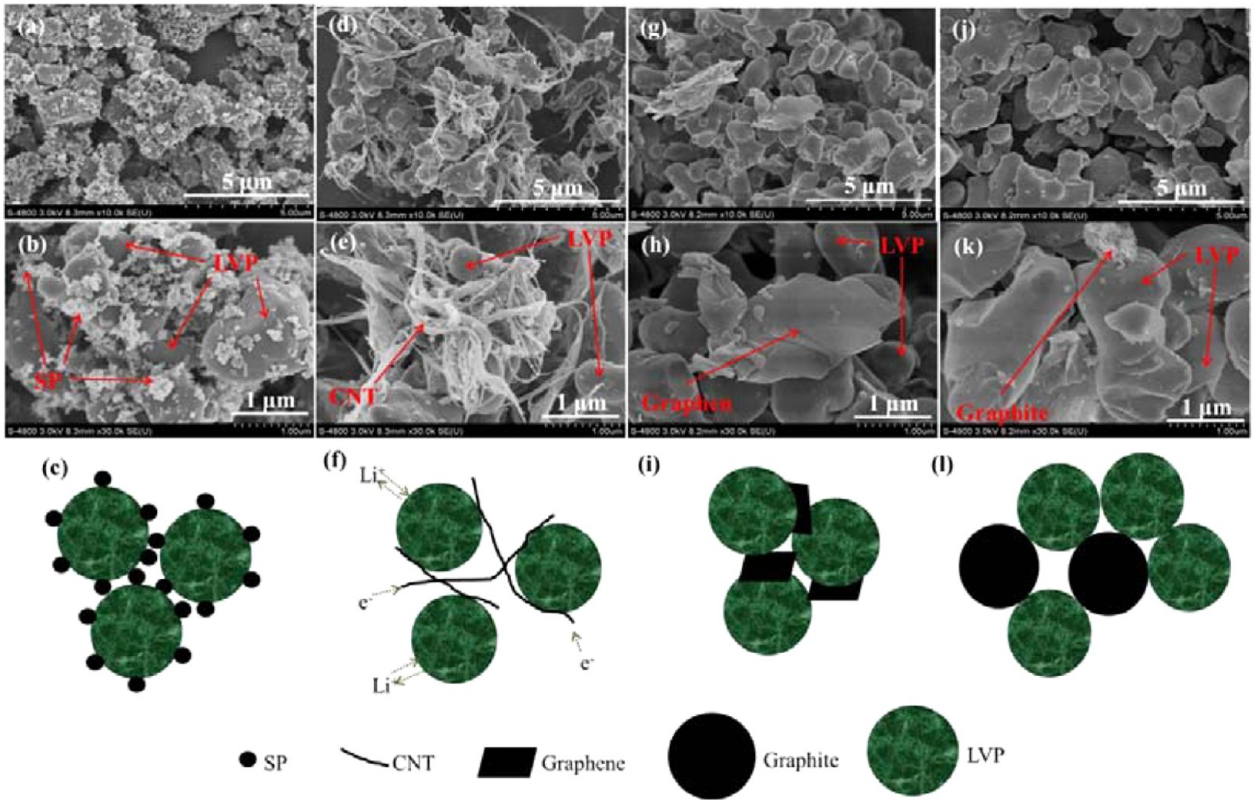

Figure 2. SEM images of LVP@SP (a and b), LVP@CNT (d and e), LVP@Graphene (g and h), and LVP@Graphite (j and k) and schematic illustrations of LVP@SP (c), LVP@CNT (f), LVP@Graphene (i), and LVP@Graphite (l).

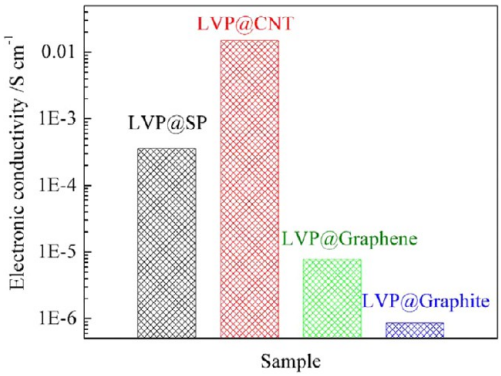

Figure 3. Electronic conductivities of LVP@SP, LVP@CNT, LVP@Graphene, and LVP@Graphite.

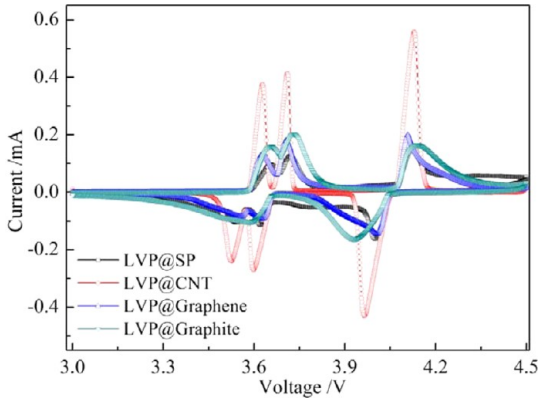

Figure 4. CV curves of LVP@SP, LVP@CNT, LVP@Graphene, and LVP@Graphite at a scan rate of 0.1 mV s^{-1}.

carbon can act both as a reducing agent and a carbon source. A strong connection between the LVP and carbon can be formed in this synthesis process. So, a better electron transportation pathway between the LVP and carbon can be formed. Second, when a large amount of LVP particles are well distributed in the carbon network, the interconnected carbon framework can provide a good conductive matrix for the hybrid material, which will largely improve the overall electronic conductivity.

A significant difference in these four samples is the interconnection between the carbon components in the hybrid material. A well-connected conductive matrix can be observed in the LVP@CNT sample (Figure 2f), while a poor or incomplete connection between the carbon components can be seen in the other three samples (Figure 2c,i,l). Better connections between the LVP particle and the carbon conductive framework and the connection between different parts of the carbon conductive agents are both important. For LVP@SP, LVP@Graphene, and LVP@Graphite, the carbon conductive networks may be poorly connected, while the CNTs can be well-connected among each other and form a good conductive network in the hybrid material. So, a higher electronic conductivity may be obtained in LVP@CNT.

To confirm our deduction, the electronic conductivities of the four composites are tested. As shown in Figure 3, LVP@CNT exhibits an electronic conductivity of 1.5×10^{-2} S cm^{-1}, which is higher than 1×10^{-5} S cm^{-1} of the carbon-coated LVP in our previous work[31] and 10^{-2}–10^{-3} S cm^{-1} of a recent publication.[26] LVP@SP and LVP@Graphene present lower electronic conductivities of 3.6×10^{-4} and 7.8×10^{-6} S cm^{-1}, and LVP@Graphite exhibits the lowest electronic conductivity of 8.6×10^{-7} S cm^{-1}. According to a previous report,[32] the

DOI: 10.1021/acsami.5b02242
ACS Appl. Mater. Interfaces 2015, 7, 12057−12066

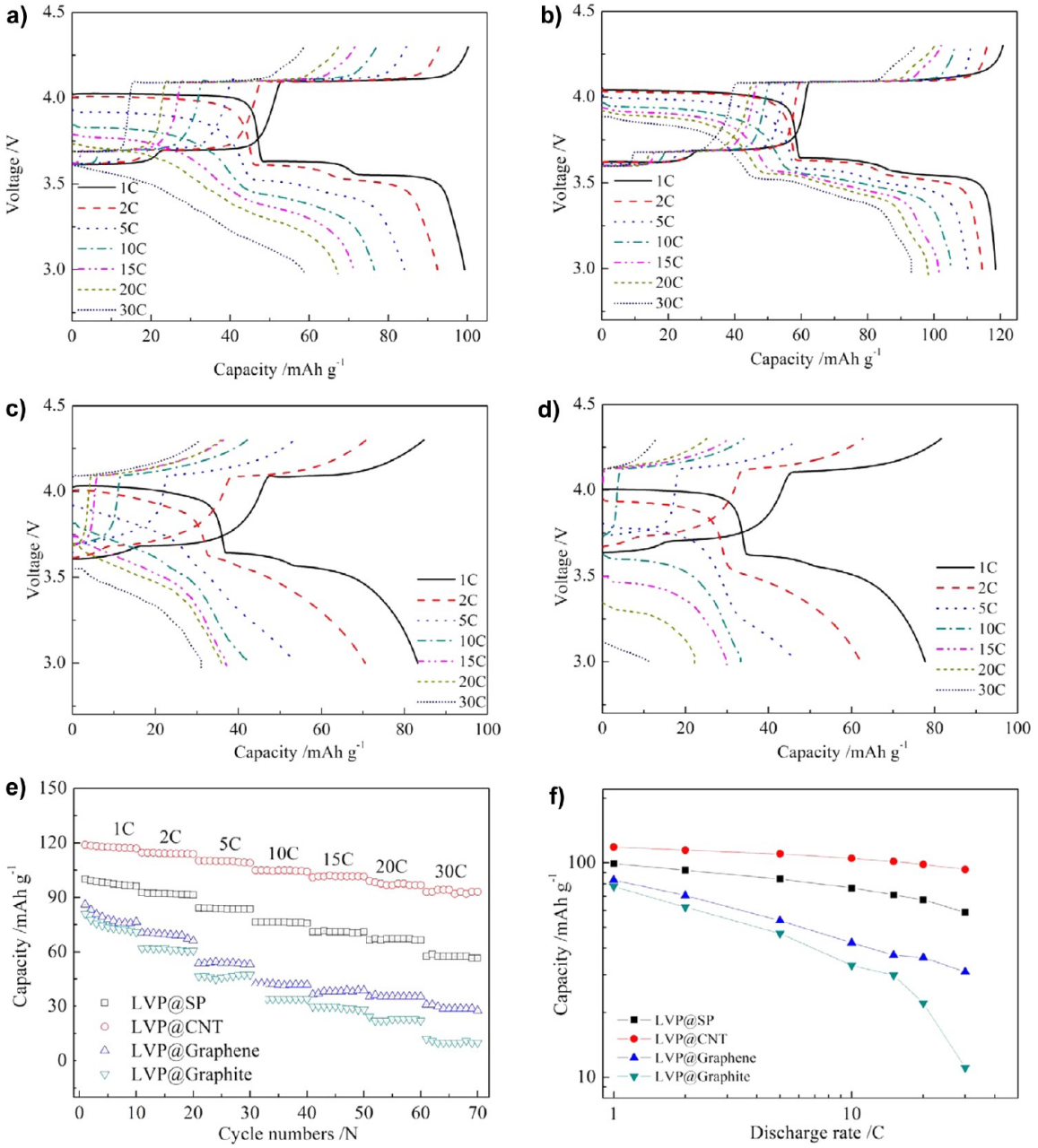

Figure 5. Charge/discharge curves of LVP@SP (a), LVP@CNT (b), LVP@Graphene (c), and LVP@Graphite (d) with different discharge rates from 1C to 2C, 5C, 10C, 15C, 20C, and 30C and the corresponding rate performances (e and f).

electronic conductivities for SP, CNT, graphene, and graphite are 0.1−1.0 S cm^{-1}, and these values are much higher than that of LVP@C in our work. As we all know, the electronic conductivity of power not only is related to its intrinsic properties but also is highly affected by the number of particle contracts. In this work, LVP@CNT presents the highest electronic conductivity (~10^{-2} S cm^{-1}) among all four samples, which is close to the pure CNT electronic conductivity (10^{-1} S cm^{-1}). This means that the CNT in LVP@CNT composites contracted closely and interconnected because of its 1D structure. LVP@SP presents the second highest electronic conductivity (~10^{-4} S cm^{-1}), which is lower than 10^{-2} S cm^{-1} of LVP@CNT but higher than 10^{-6}−10^{-7} S cm^{-1} of LVP@Graphene and LVP@Graphite. The reason may be related to the 0D structure of the SP particles. The 0D structure can increase the LVP@SP conductivity through SP particle-to-particle contract, but the 0D SP particles lack an interconnection effect, which may decrease its conductivity. The electronic conductivities for LVP@Graphene and LVP@Graphite are extremely small (10^{-6}−10^{-7} S cm^{-1}) compared to those of pure graphene and graphite (0.1−1.0 S cm^{-1}) and are close to that of pristine LVP (10^{-8} S cm^{-1}),[33] which indicates that the electronic conductivities of these two samples mainly come from the LVP and the graphene and graphite do not form an interconnection between each other.

Figure 4 shows the CV curves of the LVP@SP, LVP@CNT, LVP@Graphene, and LVP@Graphite samples. Each sample shows a similar shape, presenting three redox couple peaks, although the two reduction peaks between 3.5 and 3.7 V merged into one peak for LVP@Graphite. The three oxidation peaks at 3.6, 3.7, and 4.1 V correspond to the delithiation process and the formation of a series of transition phases of

DOI: 10.1021/acsami.5b02242
ACS Appl. Mater. Interfaces 2015, 7, 12057−12066

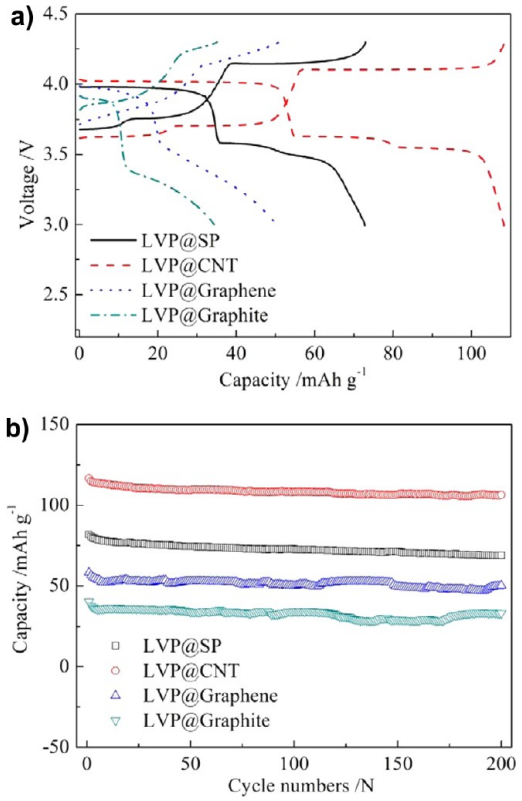

Figure 6. Charge/discharge curves (a) and corresponding cycling performances (b) of LVP@SP, LVP@CNT, LVP@Graphene, and LVP@Graphite at 5C rate.

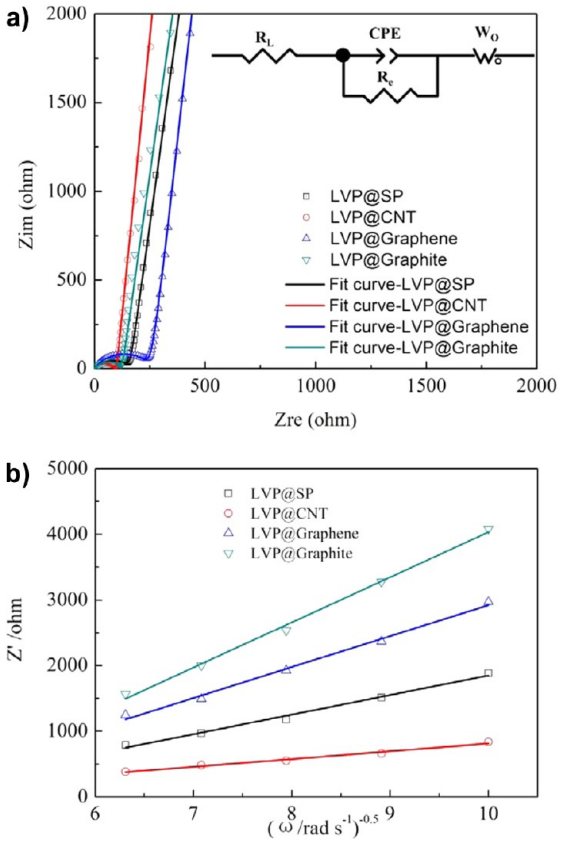

Figure 7. Nyquist plots, equivalent circuit, and fitting curves of LVP@SP, LVP@CNT, LVP@Graphene, and LVP@Graphite at the initial state (a) and the corresponding profile of the relationship between Z' and $\omega^{-1/2}$ (b).

Table 2. EIS Parameters of LVP@SP, LVP@CNT, LVP@Graphene, and LVP@Graphite

	LVP@SP	LVP@CNT	LVP@Graphene	LVP@Graphite
R_e (Ω)	161.8	85.1	213.6	126.4
R_L (Ω)	2.7	3.6	3.1	2.3

$Li_xV_2(PO_4)_3$ from x = 3.0 to 2.5, 2.0, and 1.0, respectively. It should be noted that extraction of the first lithium ion is divided into two steps because of the existence of an ordered phase $Li_{2.5}V_2(PO_4)_3$ at mixed V^{3+}/V^{4+} valence states. Three lithium ions in $Li_xV_2(PO_4)_3$ accompanied the phase transitions of $Li_xV_2(PO_4)_3$ at x = 1.0 to 2.0, 2.5, and 3.0. It can be clearly observed that LVP@CNT has the largest curve area, highest redox current, and most symmetrical and clearest splitting anodic/cathodic peaks, which indicates that it has the best electrochemical performance among all four samples. Although LVP@SP and LVP@Graphene have similar peak potentials, the poorer peak separation and symmetry are presented. For LVP@Graphite, the worst peak separation and symmetry are exhibited, and the reduction peaks between 3.5 and 3.7 V merge into one, which means that it has the worst electrochemical performance. As we all know, the peak current, peak area, peak potential, and peak symmetry are highly related to the electrochemical performances of the electrode materials. For the four samples, one of the biggest differences is the carbon materials in LVP@C. Therefore, we can conclude that the carbon types have a huge influence on the electrochemical performances of LVP@C composites.

Figure 5 shows the charge/discharge curves and corresponding rate performances of LVP@SP, LVP@CNT, LVP@Graphene, and LVP@Graphite with 1C rate charge and different discharge rates from 1C, 2C, 5C, 10C, 15C, 20C, to 30C. For the 1C rate charge/discharge profiles, three distinct plateaus can be observed for the four samples, indicating three steps of the lithiation/delithiation process, which are in good agreement with the redox peaks in the CV curves in Figure 4. For the charge/discharge curves in the four samples, the charge voltage plateaus are almost stable because the charge rates are the same, while the discharge voltage plateaus decrease with increasing discharge rate, which may be related to the high polarization at high rate. Except for LVP@CNT (Figure 5b), the other three laminates do not show all three plateaus at higher rate, which implies that an incomplete Li^+ insertion/delithiation process occurred at high rate in these three samples. For example, at 30C rate, LVP@CNT exhibited three voltage plateaus, while the other three samples showed a slope, indicating the incomplete lithiation/delithiation process of LVP@SP, LVP@Graphene, and LVP@Graphite. What is more, at 30C rate, the discharge voltage starts from 3.85 V for LVP@CNT, from 3.60 V for LVP@SP, from 3.55 V for LVP@Graphene, and from 3.15 V for LVP@Graphite, which means that LVP@CNT has the lowest polarization and best electrochemical performance among the four samples. Because all laminates were prepared at the same conditions and therefore have comparable ionic transport characteristics, the incomplete lithiation/delithiation and high polarization in the latter three laminates at high rate indicate that the performance is hindered by the poor electron transportation. The well-connected conductive nanotube matrix in LVP@CNT helps

DOI: 10.1021/acsami.5b02242
ACS Appl. Mater. Interfaces 2015, 7, 12057−12066

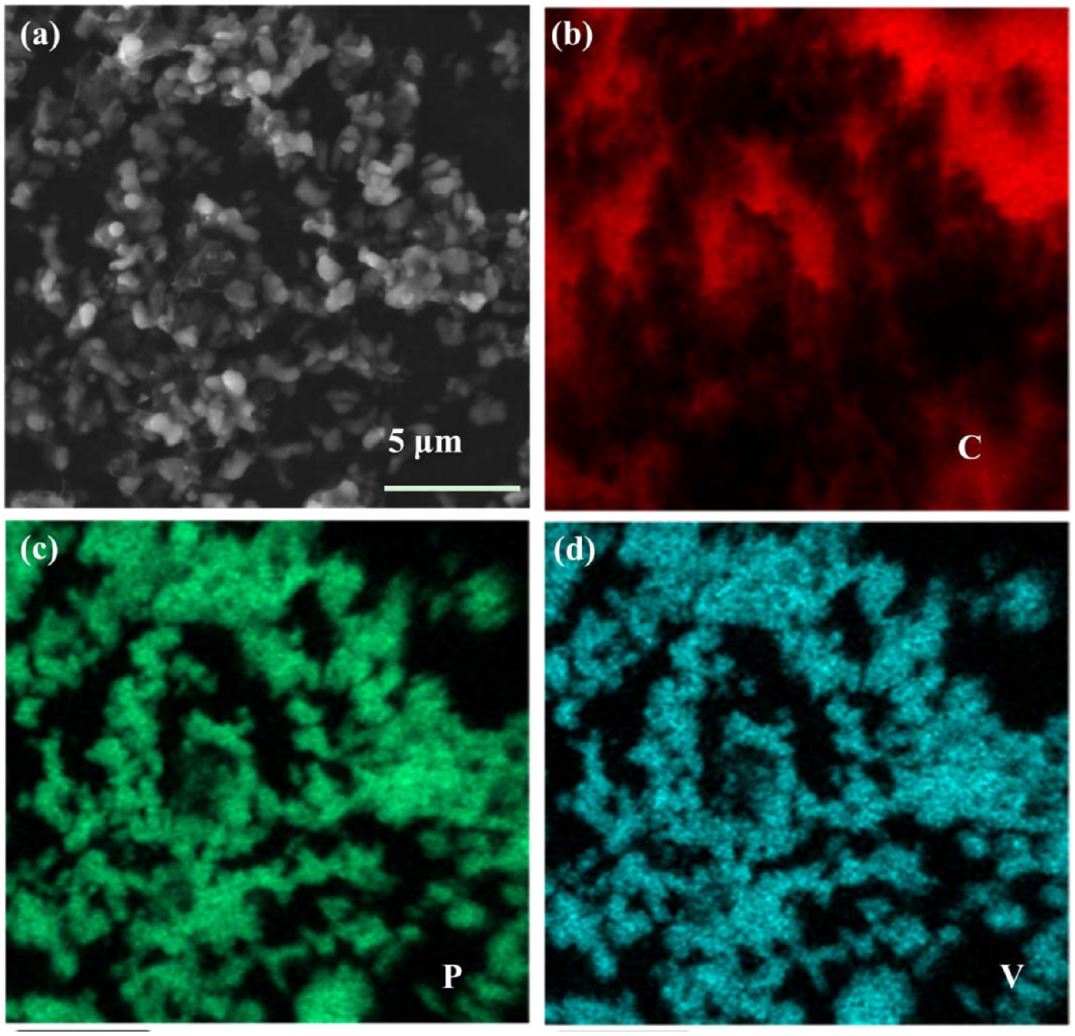

Figure 8. SEM image (a) and EDS mappings of C (b), P (c), and V (d) of LVP@CNT composites.

one to achieve a superior rate performance, while the disconnected conductive carbon compounds in LVP@SP, LVP@Graphene, and LVP@Graphite cannot provide enough conductive pathway for charge transportation, as we suggested in the former discussion (Figure 3).

The capacities also have huge differences for these four laminates (Figure 5e,f). Even at a low rate of 1C, the discharge capacity of LVP@CNT is 118.52 mAh g^{-1}, which is 89.11% of its theoretical capacity (133 mAh g^{-1}), while only 99.29, 83.19, and 77.72 mAh g^{-1} capacities can be obtained for LVP@SP, LVP@Graphene, and LVP@Graphite. The difference is bigger at high rate. At 30C rate, a 93.13 mAh g^{-1} discharge capacity was obtained in LVP@CNT, which is 78.58% of the capacity at 1C (118.52 mAh g^{-1}), while in the LVP@SP, LVP@Graphene, and LVP@Graphite, only 59.17%, 37.28%, and 14.26% of their 1C capacities could be obtained at a 30C rate, which were 58.75, 31.01, and 11.09 mAh g^{-1}, respectively. The difference in the rate performance demonstrates the importance of the conductive network in LVP, and the proper choice of carbon compounds is crucial in high-performance LVP cathodes.

The long-term cycling performances of LVP@SP, LVP@CNT, LVP@Graphene, and LVP@Graphite are also investigated. Figure 6 shows the charge/discharge profiles and corresponding cycling performances of all of the samples at 5C charge/discharge rate. The initial discharge capacity for the LVP@CNT sample is 116.59 mAh g^{-1}, much higher than 81.81 mAh g^{-1} for LVP@SP, 58.30 mAh g^{-1} for LVP@Graphene, and 40.23 mAh g^{-1} for LVP@Graphite, respectively. This indicates insufficient lithiation for the latter three samples when cycling at 5C, which was discussed in the previous section. The results indicated that LVP@CNT shows the best rate capability and cycling performance among all of the samples. Although the capacities for the four samples are significantly different, all of the composites exhibit similar stable cycling performances. After 200 cycles, the capacity retention ratios are 91.28%, 84.23%, 86.30%, and 82.13% for LVP@CNT, LVP@SP, LVP@graphene, and LVP@graphite, respectively. This indicates that the LVP has a good cycling performance even at partial charge and discharge for long cycles. According the previous reports,[26,29] the structure of LVP is very stable and can undergo long-term cycling. The four as-synthesized samples have the same $P2_1/n$ structure and similar cell parameters (Table 1), which makes them exhibit the similar capacity retention over 200 cycles.

Electron impact spectroscopy (EIS) measurement is employed to further analyze how the carbon dimensions affect the electrochemical performances of LVP@C composites. All of the cells were tested at a discharge state after five formation cycles. As shown in Figure 7, all of the samples show a semicircle in the high-frequency region and a straight line in the

DOI: 10.1021/acsami.5b02242
ACS Appl. Mater. Interfaces 2015, 7, 12057−12066

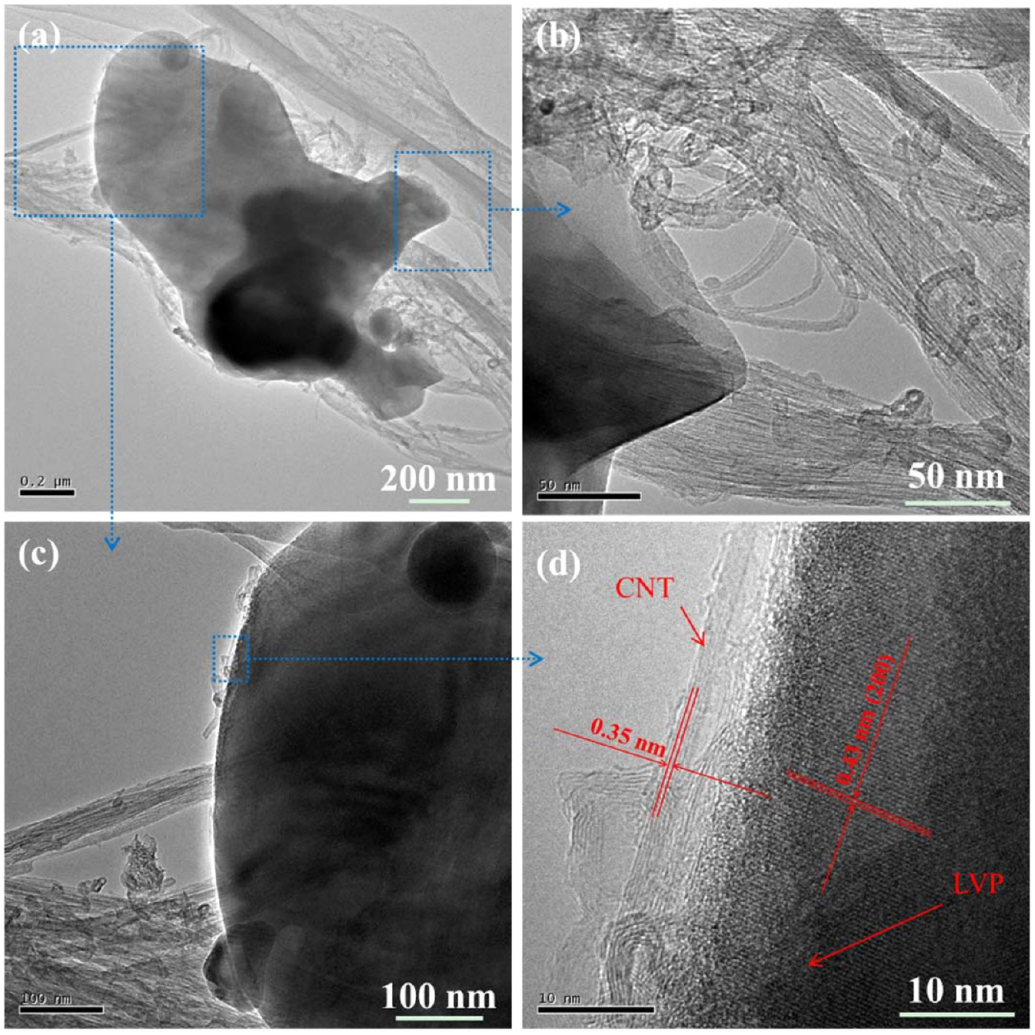

Figure 9. TEM images (a–d) of LVP@CNT composites at different magnifications.

low-frequency region. The small intercept at the Z_{re} axis corresponds to the cell ohmic resistance (R_L), which includes the LVP@C electrode, separator, lithium counter electrode, and cell hardware. The total amount of this resistance (R_L) for the four samples is very similar, and it is very small and can be neglected compared with R_e. The semicircle in the high-frequency region can be ascribed to the active-material particle-to-particle contact resistance (R_e).[34] As summarized in Table 2, the particle-to-particle contract residence (R_e) changes from 85.1 Ω for LVP@CNT to 213.6 Ω for LVP@Graphene, indicating that the carbon dimensions have a significant effect on the LVP@C samples, which further affect their electrochemical performances. As we all know, the electrochemical performance of the electrode material is closely related to several factors: the internal charge-transport resistance, lithium diffusion distance D_{Li^+} in the active-material particle, the ionic conductivity of Li^+ ion transport in the electrolyte, etc. For LVP@C in this case, the particle contract residence (R_e) of LVP@CNT is much smaller than those of the other three samples, which are 67.33%, 52.60%, and 39.84% of the resistance of LVP@Graphite, LVP@SP, and LVP@Graphene, respectively. We can see that the significantly different R_e processes may affect the electrochemical performances of the four samples, which might be the reason for the good electrochemical performance of LVP@CNT compared to the other three samples.

The straight line in the low-frequency region is attributed to the Warburg diffusion (W_s) of lithium ions into the bulk electrode material, which is evidenced by the linear relationship between Z_{re} and $\omega^{-1/2}$ (Figure 7b). By comparing the slopes of the fitting lines,[35] named the Warburg factors, we can determine the lithium-ion diffusion coefficient value (D_{Li^+}). D_{Li^+} for LVP@CNT is the highest, followed by LVP@SP and LVP@Graphene, and D_{Li^+} for LVP@Graphite is the smallest. This indicates that LVP@CNT has the best Li^+-ion diffusion property through both the electrode/electrolyte interface and bulk electrode material.

Except D_{Li^+}, the particle size, which is highly related to the lithium-ion diffusion distance (L), is also very important for electrode materials. Therefore, the particle distributions for the four samples are analyzed: LVP@CNT has the smallest particle size of 0.77 μm, followed by 1.01 μm for LVP@SP and 1.09 μm for LVP@Graphene, and LVP@Graphite has the largest particle size of 2.15 μm. The reasons for the different particle sizes of the four samples may be related to the introduction of different carbons. According to the diffusion formula $t = L^2/D$ (where t is the diffusion time, L is the ion diffusion length, and D is the ion diffusion coefficient), LVP@CNT has the highest D_{Li^+} value and the shortest L, which makes it have the fastest

DOI: 10.1021/acsami.5b02242
ACS Appl. Mater. Interfaces 2015, 7, 12057–12066

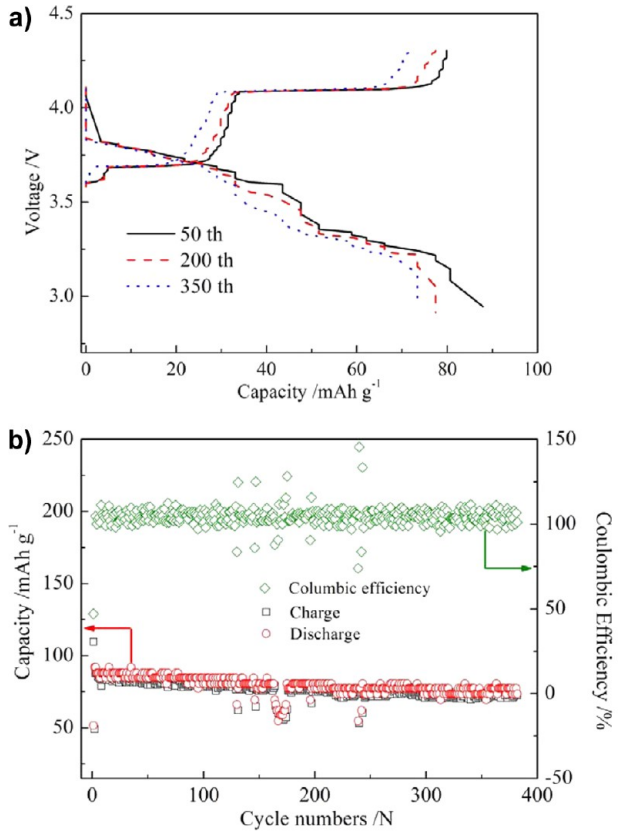

Figure 10. Charge/discharge curves (a) and corresponding cycling performance (b) of LVP@CNT at 5 C charge and 100 C discharge rates.

Table 3. Electrochemical Performances of LVP in Recent Publications

loading (mg cm^{-2})	rate	capacity (mAh g^{-1})	reference
~2.5	100C	91.94	our work
1.5–2.0	100C	100	26
2.3–2.7	50C	106.4	36
3.1	100C	81	37
2.5–3.5	100C	66	18
4.0–4.3	50C	75.5	38
~1.5	60C	88	39

lithium-ion diffusion. As we all know, there exist two important factors that affect the performances of the electrode materials for LIBs: one is the electronic conductivity, and the other is the ionic conductivity. In this work, four kinds of carbons with different performances (parts of their electrochemical performance are shown in Figure S2 in the SI) are employed to prepare LVP@C composites. The four synthesized samples exhibit different electronic conductivities and Li^+-ion conductivities, which related to the introduction of four carbons with different dimensions. Among the four samples, the LVP@CNT composite exhibits the best electrochemical performance duo to it has the highest electronic conductivity and Li^+-ion conductivity.

A series of characterization techniques were employed to further investigate the LVP@CNT composite. As shown in the energy-dispersive spectrometry (EDS) in Figure 8, the C, P, and V are uniformly distributed in the LVP@CNT samples. TEM was also utilized to characterize the detailed structures of the LVP@CNT samples. In Figure 9a, a single LVP particle is dispersed into the CNT networks, as indicated in Figure 2e. This phenomenon can be further observed in the enlarged TEM images in Figure 9b,c. The high-resolution TEM image in Figure 9d clearly shows the LVP particle, CNTs, and boundary between the LVP particle and CNT. The lattice fringes of a LVP particle with a lattice spacing of 0.43 nm, corresponding to the spacing of the (220) crystal planes, are indicated in Figure 9d. The CNT interplanar distance was measured to be 0.35 nm, in good agreement with the (002) planes of CNTs. The strong connection between the LVP particle and CNT may be related to the in situ synthesized process that uses CNTs both as reducing agents and carbon sources. Many LVP particles combined with CNTs composed together; then the CNTs interconnected, and the electronic transmission channel between the LVP particles formed via CNT networks. These effects make LVP@CNT exhibit the best electrochemical performance among all of the LVP@C composites.

To confirm the high rate performance of the LVP@CNT composites, the charge/discharge curves and cycling performance at 5C charge and 100C discharge rates are further investigated. As shown in Figure 10, a large specific capacity of 91.94 mAh g^{-1} (69.13% of its theoretical capacity) was obtained. The reversible capacity remains 79.82% after 382 cycles, and most of the Coulombic efficiency values are close to 100% (Figure 10b). The LVP@CNT sample reported in this paper exhibits a rate capacity even at an ultrahigh discharge rate at 100C with an electrode loading of 2.5 mg cm^{-2}. The electrochemical performances of recent works[18,36−39] about LVP are summarized in Table 3; we suggest that when compared with the same rate and comparable loading, the LVP@CNT composite in this work shows the best electrochemical performance among all related work.

4. CONCLUSION

The LVP@C sample has been successfully synthesized via an in situ synthesis method using inorganic carbon as both the reducing agent and carbon source. The LVP particles are well dispersed into the inorganic carbon networks, and the carbons (SP, CNT, graphene, and graphite) maintain their original morphology. The electronic conductivity and electrochemical performance results indicated that the carbon dimensions have a significant effect on the performance of the LVP@C composite. The LVP@CNT composite shows the best electrochemical performance among all of the samples and shows high potential to be a good candidate for the new generation of cathode materials for LIBs for HEV and EV. The synthesis process and experimental results are by no means limited to the preparation of LVP or other olivine materials: They can easily be extended to any other cathode material in which we need to improve their electronic and ionic conductivities.

■ ASSOCIATED CONTENT

Ⓢ Supporting Information

Particle size distributions and charge/discharge curves. The Supporting Information is available free of charge on the ACS Publications website at DOI: 10.1021/acsami.5b02242.

■ AUTHOR INFORMATION

Corresponding Author

*E-mail: wenfengmao123@gmail.com or WMao@lbl.gov.

DOI: 10.1021/acsami.5b02242
ACS Appl. Mater. Interfaces 2015, 7, 12057−12066

Notes

The authors declare no competing financial interest.

■ ACKNOWLEDGMENTS

This work is funded by the project of the Innovative Group for High-Performance Lithium-Ion Power Batteries R&D and Industrialization of Guangdong Province (Grant 2013N079). Also, W.-f.M. and G.A. are supported by the China Scholarship Council.

■ REFERENCES

(1) Qiu, J.; Zhang, P.; Ling, M.; Li, S.; Liu, P.; Zhao, H.; Zhang, S. Photocatalytic Synthesis of TiO_2 and Reduced Graphene Oxide Nanocomposite for Lithium Ion Battery. *ACS Appl. Mater. Interfaces* **2012**, *4* (7), 3636−3642.

(2) Qiu, J.; Lai, C.; Wang, Y.; Li, S.; Zhang, S. Resilient Mesoporous TiO_2/Graphene Nanocomposite for High Rate Performance Lithium-ion Batteries. *Chem. Eng. J.* **2014**, *256*, 247−254.

(3) Goodenough, J. B.; Park, K.-S. The Li-Ion Rechargeable Battery: A Perspective. *J. Am. Chem. Soc.* **2013**, *135* (4), 1167−1176.

(4) Kim, T.-H.; Park, J.-S.; Chang, S. K.; Choi, S.; Ryu, J. H.; Song, H.-K. The Current Move of Lithium Ion Batteries Towards the Next Phase. *Adv. Energy Mater.* **2012**, *2* (7), 860−872.

(5) Gaubicher, J.; Wurm, C.; Goward, G.; Masquelier, C.; Nazar, L. Rhombohedral Form of $Li_3V_2(PO_4)_3$ as a Cathode in Li-Ion Batteries. *Chem. Mater.* **2000**, *12* (11), 3240−3242.

(6) Yin, S. C.; Grondey, H.; Strobel, P.; Huang, H.; Nazar, L. F. Charge Ordering in Lithium Vanadium Phosphates: Electrode Materials for Lithium-Ion Batteries. *J. Am. Chem. Soc.* **2003**, *125* (2), 326−327.

(7) Chen, S.; Wu, J.; Su, Z.; Deng, L. Kinetic Studies on the Synthesis of Monoclinic $Li_3V_2(PO_4)_3$ via Solid-State Reaction. *J. Phys. Chem. A* **2014**, *118* (21), 3711−3716.

(8) Han, D.-W.; Lim, S.-J.; Kim, Y.-I.; Kang, S. H.; Lee, Y. C.; Kang, Y.-M. Facile Lithium Ion Transport through Superionic Pathways Formed on the Surface of $Li_3V_2(PO_4)_3$/C for High Power Li Ion Battery. *Chem. Mater.* **2014**, *26* (12), 3644−3650.

(9) Kang, J.; Mathew, V.; Gim, J.; Kim, S.; Song, J.; Im, W. B.; Han, J.; Lee, J. Y.; Kim, J. Pyro-Synthesis of a High Rate Nano-$Li_3V_2(PO_4)_3$/C Cathode with Mixed Morphology for Advanced Li-Ion Batteries. *Sci. Rep.* **2014**, *4*.

(10) Luo, Y.; Xu, X.; Zhang, Y.; Pi, Y.; Zhao, Y.; Tian, X.; An, Q.; Wei, Q.; Mai, L. Hierarchical Carbon Decorated $Li_3V_2(PO_4)_3$ as a Bicontinuous Cathode with High-Rate Capability and Broad Temperature Adaptability. *Adv. Energy Mater.* **2014**, *4* (16), 1−8.

(11) Rui, X.; Yan, Q.; Skyllas-Kazacos, M.; Lim, T. M. $Li_3V_2(PO_4)_3$ Cathode Materials for Lithium-Ion Batteries: A Review. *J. Power Sources* **2014**, *258*, 19−38.

(12) Sarkar, S.; Mitra, S. $Li_3V_2(PO_4)_3$ Addition to the Olivine Phase: Understanding the Effect in Electrochemical Performance. *J. Phys. Chem. C* **2014**, *118* (22), 11512−11525.

(13) Wang, S.; Zhang, Z.; Deb, A.; Yang, L.; Hirano, S.-i. Synthesis, Characterization, and Electrochemical Performance of Ce-Doped Ordered Macroporous $Li_3V_2(PO_4)_3$/C Cathode Materials for Lithium Ion Batteries. *Ind. Eng. Chem. Res.* **2014**, *53*, 19525−19523.

(14) Yang, Y.; Xu, W.; Guo, R.; Liu, L.; Wang, S.; Xie, D.; Wan, Y. Synthesis and Electrochemical Properties of Zn-Doped, Carbon Coated Lithium Vanadium Phosphate Cathode Materials for Lithium-Ion Batteries. *J. Power Sources* **2014**, *269*, 15−23.

(15) Zhang, R.; Zhang, Y.; Zhu, K.; Du, F.; Fu, Q.; Yang, X.; Wang, Y.; Bie, X.; Chen, G.; Wei, Y. Carbon and RuO_2 Binary Surface Coating for the $Li_3V_2(PO_4)_3$ Cathode Material for Lithium-Ion Batteries. *ACS Appl. Mater. Interfaces* **2014**, *6* (15), 12523−12530.

(16) Wu, Y.; Zhao, X.; Song, Z.; Lin, L.; Du, C.; Tang, Z. Effect of Process Medium on the Synthesis of Carbon Coated Lithium Vanadium Phosphate Composite Using Rheological Phase Reaction Method. *J. Power Sources* **2015**, *274*, 782−790.

(17) Zhang, X.; Kuhnel, R.-S.; Schroeder, M.; Balducci, A. Revisiting $Li_3V_2(PO_4)_3$ as an Anode—An Outstanding Negative Electrode for High Power Energy Storage Devices. *J. Mater. Chem. A* **2014**, *2* (42), 17906−17913.

(18) Zhang, X.; Böckenfeld, N.; Berkemeier, F.; Balducci, A. Ionic-Liquid-Assisted Synthesis of Nanostructured and Carbon-Coated $Li_3V_2(PO_4)_3$ for High-Power Electrochemical Storage Devices. *ChemSusChem* **2014**, *7* (6), 1710−1718.

(19) Yin, S. C.; Grondey, H.; Strobel, P.; Anne, M.; Nazar, L. F. Electrochemical Property: Structure Relationships in Monoclinic $Li_{3-y}V_2(PO_4)_3$. *J. Am. Chem. Soc.* **2003**, *125* (34), 10402−10411.

(20) Ren, M. M.; Zhou, Z.; Gao, X. P.; Peng, W. X.; Wei, J. P. Core−Shell $Li_3V_2(PO_4)_3$@C Composites as Cathode Materials for Lithium-Ion Batteries. *J. Phys. Chem. C* **2008**, *112* (14), 5689−5693.

(21) Huang, H.; Yin, S. C.; Kerr, T.; Taylor, N.; Nazar, L. F. Nanostructured Composites: A High Capacity, Fast Rate $Li_3V_2(PO_4)_3$/Carbon Cathode for Rechargeable Lithium Batteries. *Adv. Mater.* **2002**, *14* (21), 1525−1528.

(22) Wang, S.; Zhang, Z.; Deb, A.; Yang, C.; Yang, L.; Hirano, S.-i. Nanostructured $Li_3V_2(PO_4)_3$/C Composite as High-Rate and Long-Life Cathode Material for Lithium Ion Batteries. *Electrochim. Acta* **2014**, *143*, 297−304.

(23) Xu, J.; Chou, S.-L.; Zhou, C.; Gu, Q.-F.; Liu, H.-K.; Dou, S.-X. Three-Dimensional-Network $Li_3V_2(PO_4)_3$/C Composite as High Rate Lithium Ion Battery Cathode Material and Its Compatibility with Ionic Liquid Electrolytes. *J. Power Sources* **2014**, *246*, 124−131.

(24) Wu, W.-l.; Liang, J.; Yan, J.; Mao, W.-f. Synthesis of $Li_3Ni_xV_{2-x}(PO_4)_3$/C Cathode Materials and Their Electrochemical Performance for Lithium Ion Batteries. *J. Solid State Electrochem.* **2013**, *17* (7), 2027−2033.

(25) Son, J. N.; Kim, S. H.; Kim, M. C.; Kim, G. J.; Aravindan, V.; Lee, Y. G.; Lee, Y. S. Superior Charge-Transfer Kinetics of NASICON-Type $Li_3V_2(PO_4)_3$ Cathodes by Multivalent Al^{3+} and Cl^- Substitutions. *Electrochim. Acta* **2013**, *97*, 210−215.

(26) Zhang, X.; Kühnel, R.-S.; Hu, H.; Eder, D.; Balducci, A. Going Nano with Protic Ionic Liquids—The Synthesis of Carbon Coated $Li_3V_2(PO_4)_3$ Nanoparticles Encapsulated in a Carbon Matrix for High Power Lithium-Ion Batteries. *Nano Energy* **2015**, *12*, 207−214.

(27) Hong, J. K.; Lee, J. H.; Oh, S. M. Effect of Carbon Additive on Electrochemical Performance of $LiCoO_2$ Composite Cathodes. *J. Power Sources* **2002**, *111* (1), 90−96.

(28) Gui, X.; Zeng, Z.; Zhu, Y.; Li, H.; Lin, Z.; Gan, Q.; Xiang, R.; Cao, A.; Tang, Z. Carbon Nanotubes: Three-Dimensional Carbon Nanotube Sponge-Array Architectures with High Energy Dissipation. *Adv. Mater.* **2014**, *26* (8), 1307−1307.

(29) Wu, Z.-S.; Ren, W.; Xu, L.; Li, F.; Cheng, H.-M. Doped Graphene Sheets as Anode Materials with Superhigh Rate and Large Capacity for Lithium Ion Batteries. *ACS Nano* **2011**, *5* (7), 5463−5471.

(30) Cheng, Y.-W.; Lin, C.-K.; Chu, Y.-C.; Abouimrane, A.; Chen, Z.; Ren, Y.; Liu, C.-P.; Tzeng, Y.; Auciello, O. Electrically Conductive Ultrananocrystalline Diamond-Coated Natural Graphite−Copper Anode for New Long Life Lithium-Ion Battery. *Adv. Mater.* **2014**, *26*, 3724−3729.

(31) Mao, W.-f.; Yan, J.; Xie, H.; Tang, Z.-y.; Xu, Q. The Interval High Rate Discharge Behavior of $Li_3V_2(PO_4)_3$/C Cathode Based on in Situ Polymerization Method. *Electrochim. Acta* **2013**, *88*, 429−435.

(32) Marinho, B.; Ghislandi, M.; Tkalya, E.; Koning, C. E.; de With, G. Electrical Conductivity of Compacts of Graphene, Multi-Wall Carbon Nanotubes, Carbon Black, and Graphite Powder. *Powder Technol.* **2012**, *221*, 351−358.

(33) Yin, S. C.; Strobel, P. S.; Grondey, H.; Nazar, L. F. $Li_{2.5}V_2(PO_4)_3$: A Room-Temperature Analogue to the Fast-Ion Conducting High-Temperature Gamma-Phase of $Li_3V_2(PO_4)_3$. *Chem. Mater.* **2004**, *16* (8), 1456−1465.

(34) Pei, B.; Jiang, Z.; Zhang, W.; Yang, Z.; Manthiram, A. Nanostructured $Li_3V_2(PO_4)_3$ Cathode Supported on Reduced Graphene Oxide for Lithium-Ion Batteries. *J. Power Sources* **2013**, *239*, 475−482.

DOI: 10.1021/acsami.5b02242
ACS Appl. Mater. Interfaces 2015, 7, 12057−12066

(35) Yuan, W.; Yan, J.; Tang, Z.; Sha, O.; Wang, J.; Mao, W.; Ma, L. Mo-Doped $Li_3V_2(PO_4)_3$/C Cathode Material with High Rate Capability and Long Term Cyclic Stability. *Electrochim. Acta* **2012**, *72* (30), 138−142.
(36) Wang, C.; Guo, Z.; Shen, W.; Zhang, A.; Xu, Q.; Liu, H.; Wang, Y. Application of Sulfur-Doped Carbon Coating on the Surface of $Li_3V_2(PO_4)_3$ Composites To Facilitate Li-Ion Storage as Cathode Materials. *J. Mater. Chem. A* **2015**, *3* (11), 6064−6072.
(37) Secchiaroli, M.; Nobili, F.; Tossici, R.; Giuli, G.; Marassi, R. Synthesis and Electrochemical Characterization of High Rate Capability $Li_3V_2(PO_4)_3$/C Prepared by Using Poly(Acrylic Acid) and D-Glucose as Carbon Sources. *J. Power Sources* **2015**, *275*, 792−798.
(38) Wang, L.; Li, X.; Tang, Z.; Zhang, X. Research on $Li_3V_2(PO_4)_3$/$Li_4Ti_5O_{12}$/C Composite Cathode Material for Lithium Ion Batteries. *Electrochem. Commun.* **2012**, *22*, 73−76.
(39) Zhang, L.; Xiang, H.; Li, Z.; Wang, H. Porous $Li_3V_2(PO_4)_3$/C Cathode with Extremely High-Rate Capacity Prepared by a Sol−Gel-Combustion Method for Fast Charging and Discharging. *J. Power Sources* **2012**, *203*, 121−125.

DOI: 10.1021/acsami.5b02242
ACS Appl. Mater. Interfaces 2015, 7, 12057−12066